Modeling and Identification of a Strip Guidance Process with Internal Feedback

Marcel P. G. J. Besteman, Camille H. L. Limpens, Robert Babuška, John B. Otten, and Michel Verhaegen, *Member, IEEE*

***Abstract*—A physically interpretable model of an experimental strip guidance installation, operated at Hoogovens Research and Development in the Netherlands, is derived by means of system identification. This process consists of an offset pivot guide steering roll with five degrees of freedom, four cylindrical guide rolls, and one driving roll. In this experimental installation, an endless steel strip is created by welding the ends of the strip to allow for continuous experimentation. As this endless strip introduces an internal mechanical feedback in the process, a closed-loop identification problem arises. Five identification strategies are applied and compared for a single operating condition, determined by the strip speed and tension, using experimental data. One of these strategies is called the controller compensation in closed-loop strategy. This new technique is proposed to reduce the closed-loop identification problem into an open-loop one by using a regulator to compensate the internal feedback due to the endless strip. From the preliminary experiments for one operating condition, this strategy is selected for further analysis as it yields the smallest prediction error. The physically interpretable model is obtained by identifying a linear time-invariant system for different operation conditions, and by expressing the model parameters in terms of geometric and kinematic parameters that characterize the strip guidance installation. The model yields improved prediction capabilities compared to other models proposed in the literature. The results presented in this paper are achieved in cooperation between Hoogovens Research and Development and the Control Laboratory at the Delft University of Technology.**

***Index Terms*—Closed-loop identification, physically interpretable modeling, strip guidance, subspace identification.**

I. Introduction

TRACKING problems in processing lines of the steel industry generally result in damage and partial rejection of the steel strip, often combined with damage to the installation and delay in the production process [1]. Preshaped rolls and steering rolls are used to reduce these tracking problems [2]. To properly control the strip guidance process by means of steering rolls, a model of this process is needed. In the literature, a first-order model of strip guidance over a cylindrical roll was proposed by Campell [3] and Shelton [4]. An extension to a second-order model of this process was suggested by Shelton [5].

Manuscript received April 30, 1996; revised February 19, 1997 and April 2, 1997. Recommended by Associate Editor, B. Lohmann.

M. P. G. J. Besteman, R. Babuška, and M. Verhaegen are with the Department of Electrical Engineering, Control Laboratory, Delft University of Technology, 2600 GA Delft, The Netherlandsl.

C. H. L. Limpens and J. B. Otten are with the Department of Research and Development, Koninklijke Hoogovens, NL-1970 CA IJmuiden, The Netherlands.

Publisher Item Identifier S 1063-6536(98)00575-2.

At Hoogovens IJmuiden, an experimental installation is used to study the strip tracking behavior in processing lines. Fig. 1 shows this experimental installation containing one steering roll and five cylindrical guide rolls. The lateral strip position is measured by six line-scan cameras. In this experimental installation an endless steel strip is created by welding the ends of the strip, which introduces an internal feedback in the process. The lateral strip position at a certain point in the experimental installation depends not only on the steering action but also on the feedback. This internal feedback is called the mechanical feedback.

However, rather than studying the strip guidance process in the experimental installation, the aim of this research was to develop a model for real processing lines. In these lines, there is no mechanical feedback, and thus the identification results obtained for the experimental installation cannot be directly applied to the processing lines. In order to transfer the results to the processing lines, a physically interpretable open-loop model of the experimental installation is needed. In our context, physical interpretability requires that the model parameters only depend on geometrical and kinematic quantities that characterize the strip guidance in process lines.

Apart from achieving the above goal, the presented results have a more general research interest. More precisely, the identification strategy followed shows that identifying physical real-life systems is far more than collecting data and applying standard "black-box" identification techniques. Contrary to this often simple-minded view on system identification, the current study does the following:

1) *Shows the importance of structuring the identification problem* at hand. In this step, the different subsystems and their relationships are highlighted, resulting in a block-schematic representation of the system. Based on this step, the type of identification problem and a class of suitable identification methods can be selected.
2) *Compares four different identification methods* which can be applied to linear systems operating in closed loop, with different feedback loops. These four methods include three existing strategies, namely the direct use of input and output data of the system when the delay of the process is sufficiently large [6], the two-stage approach [7], and the approach based on subspace identification [8]. One new technique was developed in the course of this research, called the controller compensation in closed loop (CCCL).
3) *Highlights the importance of preprocessing the measured input and output data sequences and compensating for*

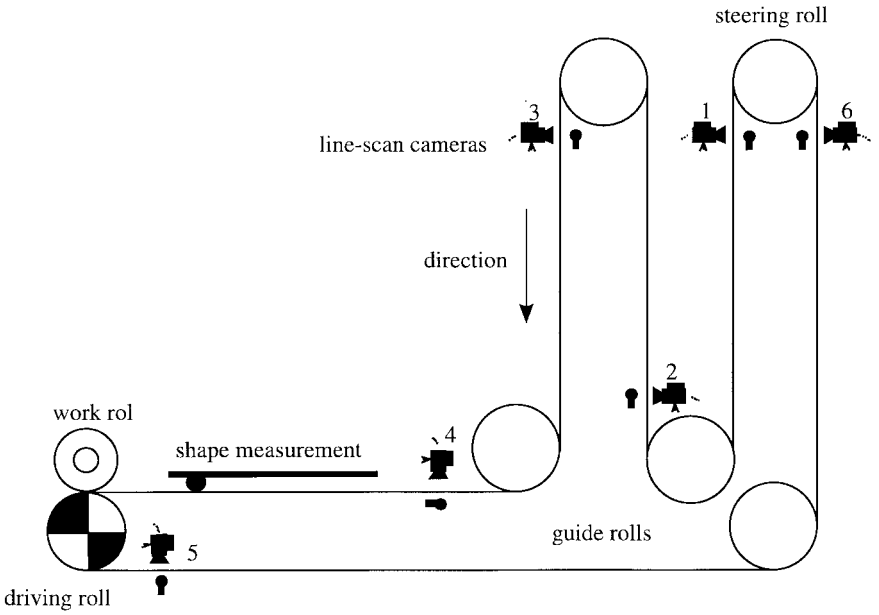

Fig. 1. The experimental installation.

deterministic trends as well as for time delays in the process.

The obtained model is validated under experimental conditions that were not considered in the process of constructing this model.

This paper is organized in eight sections: Section II presents a first-order physical model of strip guidance over cylindrical guide rolls. In Section III, the experimental installation is analyzed and a block diagram of this installation is derived. Four standard identification strategies to solve the problem are reviewed in Section IV and a new method called controller compensation in closed loop is proposed. Section V describes data collection and data preprocessing. The five identification strategies proposed in Section IV are applied to real-life data of the experimental installation in Section VI. The individual strategies are evaluated and the most accurate and reliable one is used to derive a physically interpretable model of the installation as discussed in Section VII. Section VIII concludes the paper.

II. Physical First-Order Modelling of Lateral Strip Movement

To develop equations that describe the lateral movement of a strip is a difficult task. Many factors influence the behavior of the strip, e.g., the physical properties of the strip, the nature of the surface of the strip and of the rolls, the misalignment of the rolls, friction, the mechanical rigidity, and the vibration of the machine structure. In this section, a first-order physical model for the lateral strip movement over a cylindrical roll is discussed.

Consider two parallel rolls shown in Fig. 2. When the strip moves over a perfect roll, but the wrap of the strip is skewed on the roll, the strip will move sidewise in a direction that tends to reduce the unbalanced forces which act upon the strip. The rate of sideways movement will be approximately in proportion to the angle of skew and to the velocity of the strip. Campbell [3] derived the following first-order model for the lateral strip movement over a cylindrical roll:

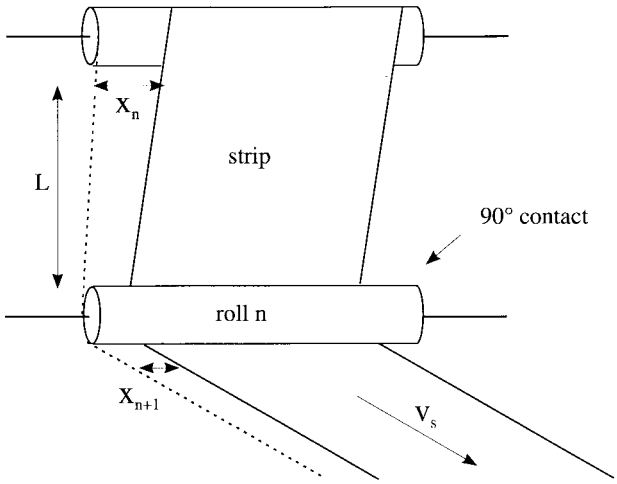

Fig. 2. Strip movement over a cylindrical roll.

$$\frac{X_{n+1}(s)}{X_n(s)} = \frac{1}{1+\tau s}, \quad \text{where } \tau = \frac{L}{v_s} \tag{1}$$

and

- $X_{n+1}(s)$ Laplace transform of the position signal just after the roll [m];
- $X_n(s)$ Laplace transform of the position signal before the roll at distance L [m];
- L distance from the point where x_n is measured to the roll [m];
- v_s strip speed [m/s].

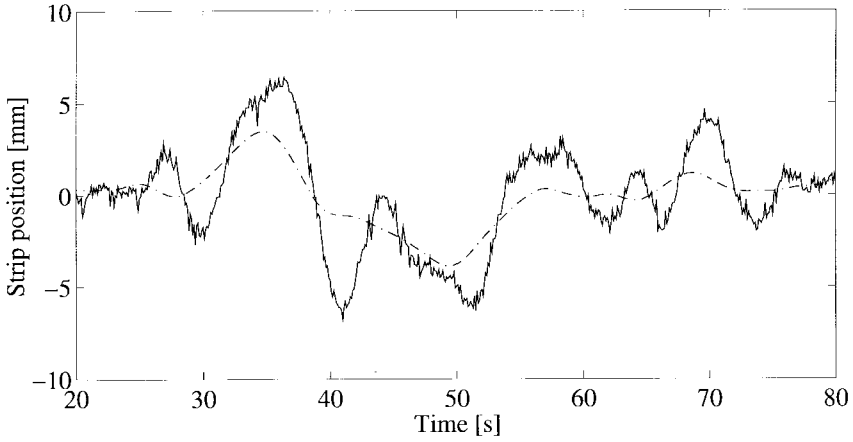

Fig. 3. Measured position at camera 5 (solid) compared with the simulated position of the model given by (3) (dashed-dotted).

The subscript n refers to the nth subprocess. Shelton [4] introduced a time delay to this model

$$T_d = \frac{L_{\text{roll}}}{v_s} \tag{2}$$

where L_{roll} is the length of the contact area between the roll and the strip (in meters). The model now becomes

$$\frac{X_{n+1}(s)}{X_n(s)} = \frac{e^{-T_d s}}{1+\tau s}. \tag{3}$$

Four of these first-order models with a delay are connected in series and applied to predict the lateral strip position at camera 5 of the experimental installation, using the actual measurement of the position at camera 1 as input. The model parameters are obtained by measurements of the necessary geometrical quantities. Fig. 3 shows the simulation results of the physical model. The actual model parameters cannot be given because of industrial confidentiality.

The performance of this model would not be satisfactory for designing a controller necessary to keep the strip in the center of the rolls. A series connection of four second-order models according to Shelton [5] gives similar unsatisfactory results. This is the reason why an open-loop model of the installation is derived by identification.

III. Modeling of the Experimental Strip Guidance Installation

In this section, the experimental installation is analyzed. By dividing the installation into subprocesses, a block diagram can be derived. The lateral strip displacements from camera 1 to camera 6 are divided into elementary subprocesses as shown in Fig. 2. Thus, the identified models can be compared with the theory according to Campell [3] and Shelton [4]. The first subprocess is from camera 1 to camera 2, the second subprocess from camera 2 to camera 3 and so on, see also Figs. 4 and 6.

Another important element of the installation is the steering roll. An offset pivot guide (OPG) steering roll [2], shown in Fig. 5, is used. The lateral strip position due to the OPG

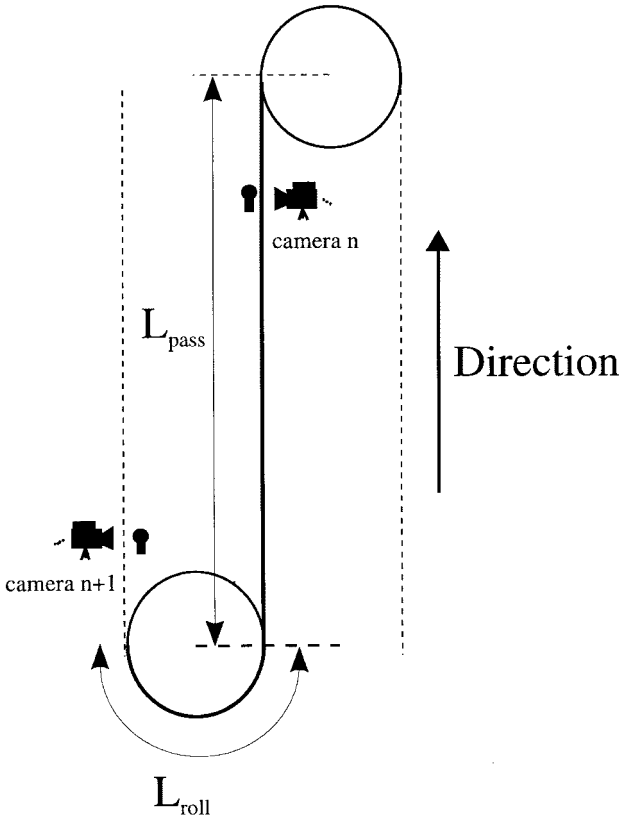

Fig. 4. A subprocess.

steering roll is expressed by

$$x(t) = x_0(t) + \Delta x(t), \quad \text{where } \Delta x(t) = L_{\text{opg}} \sin \varphi^{\text{sr}}(t) \tag{4}$$

where

$x(t)$	lateral strip position after the steering roll [m];
$x_0(t)$	lateral strip position before the steering roll [m];
$\Delta x(t)$	lateral strip displacement due to the steering roll angle [m];
$\varphi^{\text{sr}}(t)$	OPG steering roll pivot angle [rad];
L_{opg}	length of the offset pivot guide frame [m].

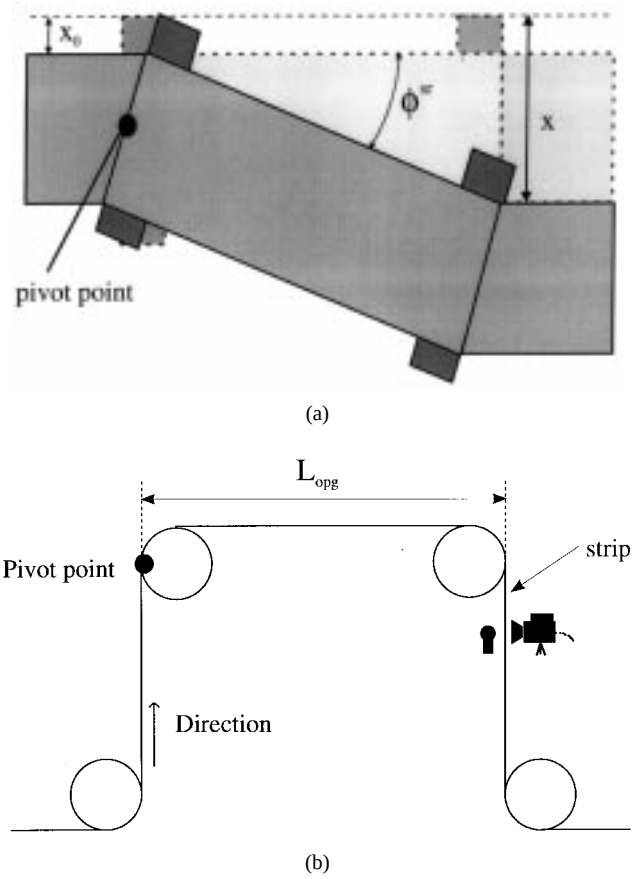

Fig. 5. The offset pivot guide steering roll. (a) Top view. (b) Side view.

Since an offset pivot guide steering roll with only one roll is used in the experimental installation, the length of the OPG frame reduces to the diameter of the steering roll. The OPG steering roll can be divided into two processes. The first process describes the transfer function from the desired OPG angle to the actual steering angle. This process contains mainly the actuator dynamics of the steering roll and is considered ideal, which means that the transfer function of this process is equal to one, i.e., the provided steering angle is equal to the actual steering angle. This consideration is verified by measurements. The second process introduces a nonlinearity to the system. This nonlinearity is given by (4) and has a negligible effect, since the steering roll angle is limited to $\pm 3°$.

There is still one process left. This is the displacement process from camera 6 via the steering roll back to camera 1. We can consider this as the mechanical feedback in the process. In Fig. 6, all subprocesses are connected together in a block diagram. An additional control loop is added which can be disconnected by switch T_1. This control loop is used to reduce the effects of disturbances in identification, as explained later on. Because of the two feedback loops in Fig. 6 a closed-loop identification method is needed to determine an open-loop model for the individual subprocesses.

Fig. 6 contains the following signals:

φ_{con}	angle computed by the controller [rad];
φ^{sr}	actual angle of the steering roll [rad];
X_1^{sr}	lateral strip displacement at camera 1 due to the steering roll angle [m];
X_1^{ml}	lateral strip position at camera 1 due to the mechanical loop [m];
X_6^{des}	desired lateral strip position at camera 6 [m];
X_n	actual lateral strip position at camera n [m];
T_1	control on/off switch;
φ^{gbn}	excitation signal (generalized binary noise) [9] [rad].

IV. Closed-Loop Identification

As shown in Fig. 6, a control loop can be added to the system. Hence, there are two possibilities to identify the process:

- identification of the installation without the control loop (switch T_1 open);
- identification of the installation with the control loop (switch T_1 closed).

In this section three identification strategies of the experimental installation *without the control loop* and two strategies of the installation *with the control loop* are discussed.

A. Identification of the Installation Without the Control Loop (Switch T_1 Open)

An advantage of the identification without the control loop is the reduction of the block diagram of Fig. 6 to a single-loop problem. Standard techniques can be applied to solve this problem. The first strategy discussed is an open-loop one.

Method 1—Open-Loop Identification: According to [6], open-loop identification techniques can be applied to a closed-loop system if the discrete-time delay n_k of the process is greater than the order of the system. Hence, a model of subprocess n is obtained by identifying the following subsystem:

$$x_{n+1}(k) = G_n(q)x_n(k) + H_n(q)e_0(k) \tag{5}$$

with

$x_n(k)$	input signal of subprocess n;
$x_{n+1}(k)$	output signal of subprocess n;
$G_n(q)$	transfer function of subprocess n;
$H_n(q)$	noise model of subprocess n;
$e_0(k)$	zero-mean white noise process.

The argument k denotes discrete time.

Method 2—State-Space Identification by MOESP: The second strategy requires redrawing the process P of Fig. 6 to a single-input, multiple-output (SIMO) structure shown in Fig. 7. In this structure, the multivariable output error state space-past input (MOESP-PI) scheme [8] can be applied to estimate the open-loop subprocesses from x_1^{sr} [obtained by $x_1^{\text{sr}} = 2R\sin\varphi^{\text{gbn}}$, see (4)] to the positions x_i, for $i = 1, 2, \cdots, 6$ of the remaining cameras in the first step. In the next step, noise-free signals x_i, $i = 1, 2, \cdots, 6$ are reconstructed from the obtained models. The subprocesses are identified between the noise-free signals x_i and x_{i+1}, for $i = 1, 2, \cdots, 5$ with open-loop techniques in the last step.

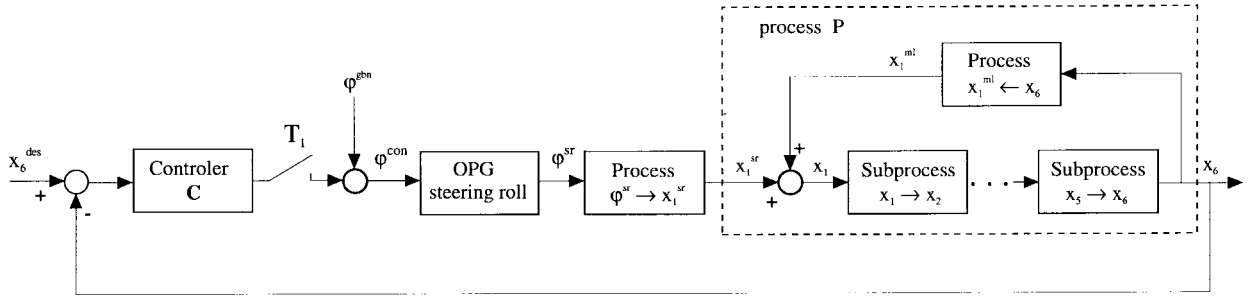

Fig. 6. Closed-loop system with process P and controller C.

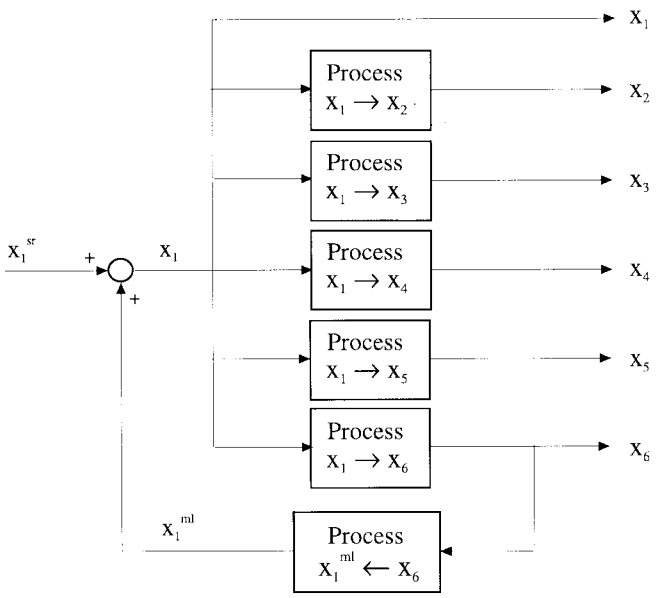

Fig. 7. Process P rewritten in a parallel structure.

Method 3—Two-Stage Method: The third strategy for identification without the control loop is the two-stage method [7]. In the first stage, the noise-free signal of camera 1 is reconstructed by identifying the sensitivity function S of the closed-loop system of Fig. 6

$$S = \frac{1}{1 + G_1 G_2 \cdots G_6}. \tag{6}$$

In the second step, a model of the first subprocess is obtained by estimating the process between the reconstructed noise-free signal of camera 1 and the measured signal of camera 2. Then, the second subprocess can be identified, etc.

The essential difference between method 2 (MOESP) and method 3 (two-stage method) is that the two-stage technique must be applied to the subprocesses sequentially, while MOESP identifies the subsystems in a parallel structure, avoiding accumulation of errors.

B. Identification of the Installation with the Control Loop (Switch T_1 Closed)

A disadvantage of experiments without the control loop is the presence of a deterministic disturbance due to the strip weld. This disturbance can cause biased estimates. The next section presents two identification strategies which need experiments with the control loop. The advantage of experiments with the control loop is the absence of a deterministic disturbance due to the strip weld, as discussed in more detail in Section V.

Method 4—Two-Stage Method Applied to Two Closed Loops: The first strategy for identification of the experimental installation with the additional control loop active (see Fig. 6) is the two-stage method [7] applied to a system with two closed loops. These loops are the control loop (outer loop) and the mechanical feedback loop (inner loop). In the first step, the sensitivity function $\hat{S}_1$ of the outer control loop is estimated. Next, the noise-free signal X_1^{sr} is reconstructed by

$$\hat{X}_1^{\mathrm{sr}} = 2R \sin \hat{\varphi}^{\mathrm{sr}} \quad \text{where } \hat{\varphi}^{\mathrm{sr}} = \hat{S}_1 \varphi^{\mathrm{gbn}}. \tag{7}$$

In the second step, a noise free signal x_1 is constructed by identifying the sensitivity function $\hat{S}_2$ of the inner loop. With this noise-free signal the individual subprocesses are identified in an open-loop way according to strategy 1.

Method 5: Controller Compensation in Closed Loop: The last strategy is called controller compensation in closed loop (CCCL) [10]. The control loop is used to compensate the internal feedback loop. When the control loop and the internal feedback loop are equal, the subprocesses can be identified consistently in an open-loop way. A process with an internal feedback is considered as shown in Fig. 8.

The output of the system is given by

$$y(k) = G_0(q)u(k) + H_0(q)e_0(k) \tag{8}$$

with

$y(k)$	output signal of the process;
$u(k)$	input signal of the process;
$e_0(k)$	zero-mean white noise.

The input signal $u(k)$ of the process $G_0(q)$ is

$$u(k) = r(k) + (F_0(q) - C(q))y(k) - F_0(q)H_0(q)e_0(k). \tag{9}$$

Defining the difference transfer function $\delta(q)$ of the control loop $C(q)$ and the internal feedback $F_0(q)$ as

$$\delta(q) = C(q) - F_0(q) \tag{10}$$

and substituting (9) and (10) into (8), an open-loop expression of the system can be derived

$$\begin{aligned} y(k) &= \frac{G_0(q)}{1 + G_0(q)\delta(q)} r(k) + \frac{1 - G_0(q)F_0(q)}{1 + G_0(q)\delta(q)} H_0(q)e_0(k) \\ &= \tilde{G}(q)r(k) + \tilde{H}(q)e_0(k). \end{aligned} \tag{11}$$

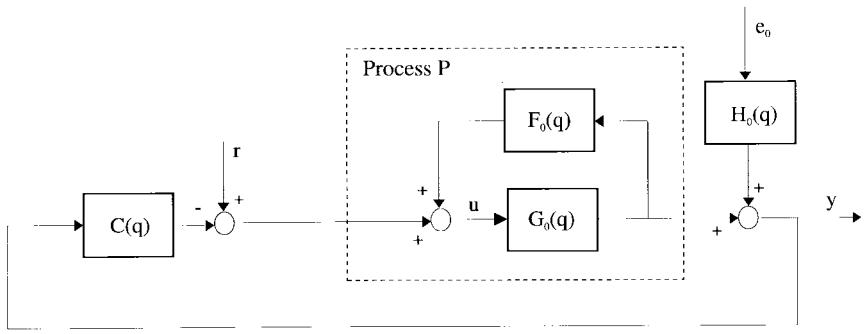

Fig. 8. System with internal feedback and an additional control loop.

The transfer function $\tilde{G}(q)$ can be decomposed as

$$\tilde{G}(q) = G_0(q)\left(1 - \frac{\delta(q)G_0(q)}{1+\delta(q)G_0(q)}\right) = G_0(q)(1-\epsilon(q)). \tag{12}$$

Here $\epsilon(q)$ is an error term which equals zero when the control loop and the internal feedback are exactly the same. Theorem 4.1 states the situation in which open-loop identification of the process G_0 in Fig. 8 is allowed.

Theorem 4.1 (CCCL): Consider the system of Fig. 8. If the following conditions are satisfied:

1) $G_0(q)$ is stable;
2) $\delta(q) = C(q) - F_0(q) = 0,\ \forall q$;
3) $r(k)$ is persistently exciting of sufficient order;

then $G_0(q)$ can be identified consistently from $r(k)$ and $y(k)$ using

$$y(k) = G_0(q)r(k) + H_0(q)(1 - G_0(q)F_0(q))e_0(k). \tag{13}$$

Proof: The proof follows directly by substituting $\delta(q) = 0$ in (11). □

In the ideal situation of Theorem 4.1, the error term $\epsilon(q)$ in (12) equals zero. Since in practice this will hold only approximately, it is useful to estimate this error term from the experimental data, as stated in Lemma 4.2.

Lemma 4.2 (Normalized Error Function): Let $\Phi_{rr}(\omega)$ be the auto-spectral density function of $r(k)$, let $\Phi_{ru}(\omega)$ be the cross-spectral density function of $r(k)$ and $u(k)$ and let $r(k)$ and $e_0(k)$ be statistically independent. An estimate of the *normalized error function* $\epsilon(e^{j\omega})$ is given by

$$\epsilon(e^{j\omega}) = \frac{\Phi_{rr}(\omega) - \Phi_{ru}(\omega)}{\Phi_{rr}(\omega)}. \tag{14}$$

Proof: In the frequency domain, the error term $\epsilon(q)$ from (12) is given by

$$\epsilon(e^{j\omega}) = \frac{\delta(e^{j\omega})G_0(e^{j\omega})}{1+\delta(e^{j\omega})G_0(e^{j\omega})}. \tag{15}$$

Considering the cross-spectral density of $r(k)$ and $y(k)$, by using (11) and the assumption that $e_0(k)$ and $r(k)$ are statistically independent we have

$$\Phi_{ry}(\omega) = \frac{G_0(e^{j\omega})}{1+\delta(e^{j\omega})G_0(e^{j\omega})}\Phi_{rr}(\omega). \tag{16}$$

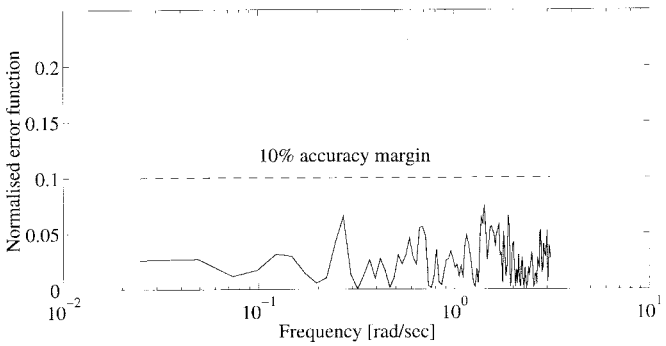

Fig. 9. Normalized error function $\epsilon(e^{j\omega})$.

By combining (15) and (16), the normalized error function is determined by

$$\epsilon(e^{j\omega}) = \delta(e^{j\omega})\frac{\Phi_{ry}(\omega)}{\Phi_{rr}(\omega)}. \tag{17}$$

Using (9), $\delta(e^{j\omega})$ can be expressed in terms of the cross-spectral density function of $r(k)$ and $u(k)$

$$\Phi_{ru}(\omega) = \Phi_{rr}(\omega) - \delta(e^{j\omega})\Phi_{ry}(\omega). \tag{18}$$

From (18) we express $\delta(e^{j\omega})$ as

$$\delta(e^{j\omega}) = \frac{\Phi_{rr}(\omega) - \Phi_{ru}(\omega)}{\Phi_{ry}(\omega)} \tag{19}$$

and substitute in (17) to obtain (14). □

In practical situations the normalized error function will never be equal to zero for all frequencies, because the internal feedback and the control loop will never be exactly the same. By adjusting the controller $C(q)$, $\delta(e^{j\omega})$ can be made as small as possible in the frequency range of interest. In this range, the real process can accurately be estimated by using open-loop identification techniques. If the normalized error function is, for example, smaller than 0.1 for all frequencies, the process is estimated with a relative accuracy of at least 10% in magnitude by using open-loop techniques. Similarly, the phase of the normalized error function can be checked. The similarity between the experimental installation and the system depicted in Fig. 8 can be seen by comparing this figure with Fig. 6, where $x_6^{\text{des}} = 0$.

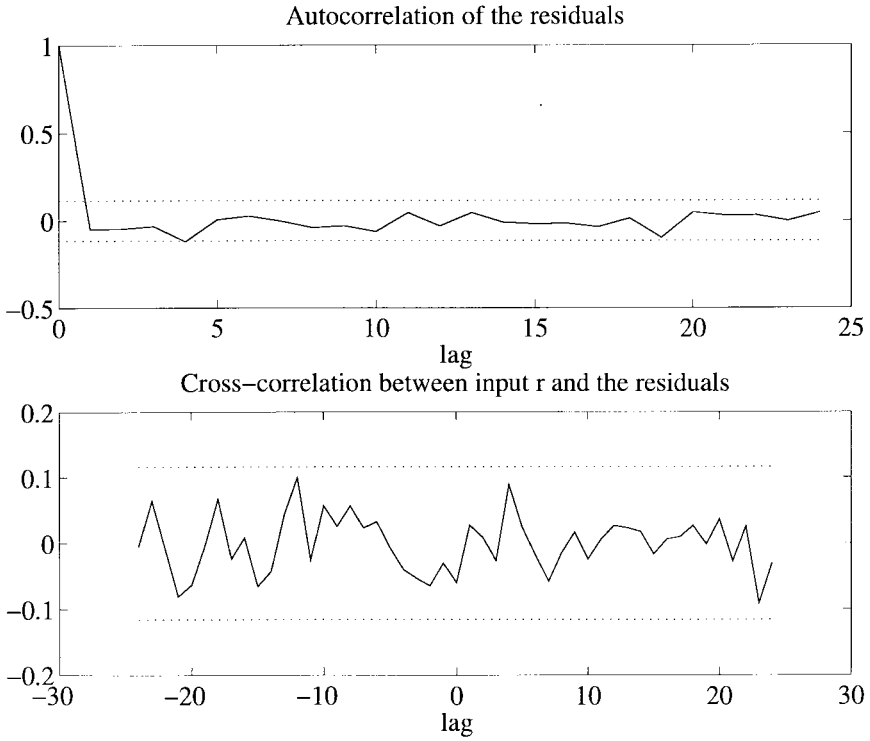

Fig. 10. The residual test on a validation data set.

Simulation Example: This section presents a simulation example of a process with internal feedback. The following transfer functions of Fig. 8 are considered:

$$G_0 = \frac{0.136z^{-1}}{1 - 0.872z^{-1}}$$
$$F_0 = \frac{0.362}{1 - 0.341z^{-1} - 0.153z^{-2}}$$
$$H_0 = 1.$$

The internal feedback F_0 is considered to be known only approximately. The controller is adjusted to this internal feedback as close as possible. This can be done for instance by minimizing the following norm: $\|F_0 - C_0\|_\infty$ [11]. Although the process G_0 is stable, the controller must be stabilizing to avoid instability of the controlled system. In this example, the controller was chosen as

$$C = \frac{0.2}{1 - 0.5z^{-1}}.$$

The transfer functions G_0 and H_0 are considered to be unknown. Generalized binary noise $r(k)$ with a variance of four is used as an excitation signal for identification. $e_0(k)$ is a zero-mean normally distributed white noise with a variance of 0.25. This results in a signal-to-noise ratio of approximately 24 dB for the output $y(k)$ of the process. The length of the time sequences are equal to 1000 samples. The first 500 samples are used to identify the process and the following 500 samples are used to validate the derived model.

First, the normalized error function is determined using (14). In Fig. 9, this function is plotted with the 10% accuracy margin. From this figure one can conclude that the process can be identified with an accuracy of at least 10% in magnitude.

The standard open-loop output error (OE) identification routine from the MATLAB Identification toolbox [12] is used to identify the process $G_0(q)$. This results in the following model:

$$\hat{G}(z) = \frac{0.141z^{-1}}{1 - 0.869z^{-1}}.$$

Fig. 10 shows the residual test of the estimation based on a validation data set. The auto-correlation function of the residuals has almost white-noise behavior. It can also be seen that the input signal and the residuals are uncorrelated. Both properties of the residuals clearly indicate that an appropriate model has been identified.

V. Data Collection and Preprocessing

Data of the experimental installation are collected by a multitasking computer system. Only the camera signals and the pivot angle are used to identify the subprocesses. The camera signals are analog signals, converted to discrete sequences by an A/D converter. The accuracy of the camera signals is 0.3 mm on a measurement range of 150 mm.

To obtain data for identification of the subprocesses, the steering roll is excited by a generalized binary noise (GBN) signal [9]. The following aspects are considered for the experiment design:

- the relevant frequency range of the signals;
- the order of the subprocesses;
- the time delays in the process;
- the static gain and the bandwidth of the subprocesses.

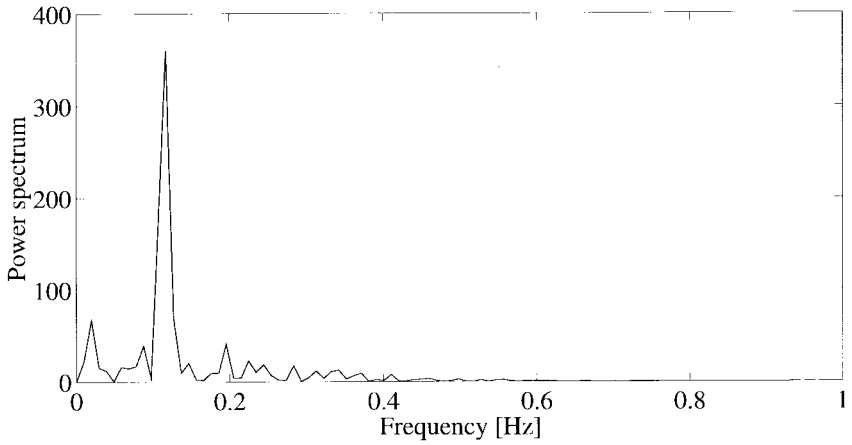

Fig. 11. The spectral density function of the signal x_2.

A. Frequency Range of the Signals

A switching probability of the GBN signal of 0.5 is used to assign white noise properties to the excitation signal $\phi^{\mathrm{gbn}}(k)$ [9]. Almost every frequency from zero to the Nyquist frequency is present in this signal.

Fig. 11 shows the frequency content of the signal x_2 at camera 2. A peak appears at a particular frequency. This frequency is the revolution frequency of the strip through the installation. The peak is due to the strip weld and can be considered as a deterministic disturbance which can cause biased estimates.

A simple method to filter this disturbance is to cut off the peak to a predefined level, keeping the phase unchanged. After this operation the time-domain signal is derived by using the inverse Fourier transform. This filtering is quite effective but it cannot fully eliminate the deterministic disturbance. On the other hand, when the controller is active (switch T_1 closed) it can effectively suppress the sinusoidal disturbance and no filtering is not necessary.

A set of data measured on the experimental installation with the control loop active is used to determine the order of the system. The CCCL method is applied to analyze these measurements. It is assumed that the internal feedback in the system, in Fig. 8 represented by the transfer function $F_0(q)$ is compensated by the controller $C(q)$, taking the latter equal to a pure time delay. To verify this condition, the normalized error function (15) is plotted in Fig. 12 for the frequency range of interest. From this figure it can be concluded that open loop techniques for the order and delay estimation can be applied, as the error is less than 10%.

B. Order of the Subprocesses

The order of a subprocess can be determined by using the singular value test in the class of recently developed subspace model identification schemes [13]. This test finds the order by searching a gap between the singular values ordered in a descending magnitude. Fig. 13 shows the singular values obtained by identifying a model between the position signals x_1 and x_2 for 12 block rows of the Hankel matrices processed by the PI variant of the MOESP family [8]. One can clearly observe the presence of a first-order, possibly a second-order

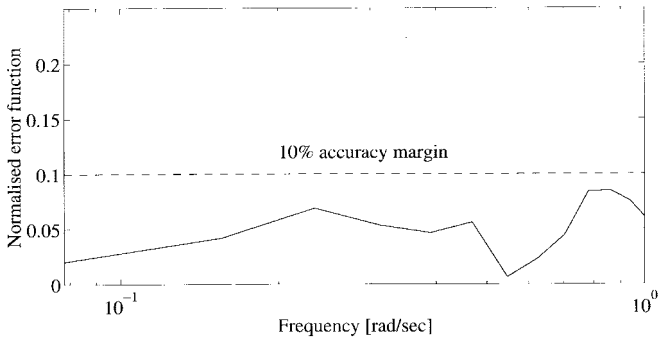

Fig. 12. The normalized error function $\epsilon(e^{j\omega})$.

dynamics. The singular value test is further combined with the prediction errors, as suggested in [13] and [8]. As the second-order model does not lead to any significant decrease of the prediction error, a first-order model is chosen.

C. Time Delays in the Process

Accurately estimating the time delay is a difficult task [14]. Three techniques are selected to estimate the time delays in the process:

- cross-correlation function between two camera signals;
- impulse responses of the subprocesses;
- minimizing a loss function.

Cross-Correlation Function: The time delay of a subprocess can be derived from a peak at the cross-correlation of two camera signals. Fig. 14 shows the cross correlation function between x_1 and x_2.

Impulse Responses of the Subprocesses: The time delay of a subprocess can also be derived by considering the impulse response. Fig. 15 shows the estimated finite impulse response of 30 lags of the first subprocess with the input signal x_1 and the output signal x_2. The time delay is estimated by finding the first nonzero parameter. The parameter number multiplied by the sample time gives the time delay. Since in Section V-B it was concluded that a first-order model is sufficient to represent the individual subprocesses, the dip in Fig. 15 is assumed to be due to noise and due to nonminimum phase dynamics, as the plot might suggest.

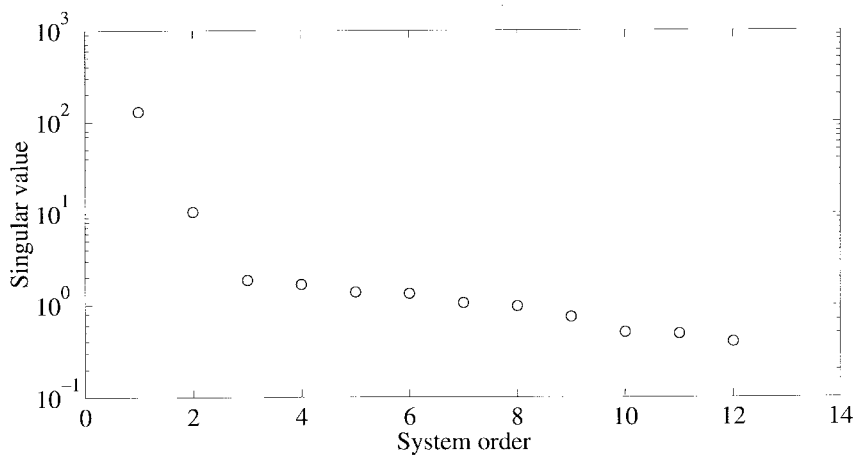

Fig. 13. The singular values with respect to the order of the first subprocess.

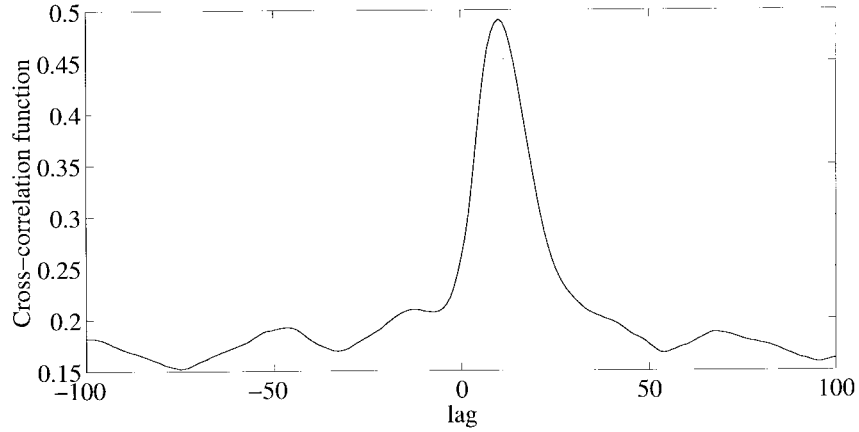

Fig. 14. Cross-correlation between x_1 and x_2.

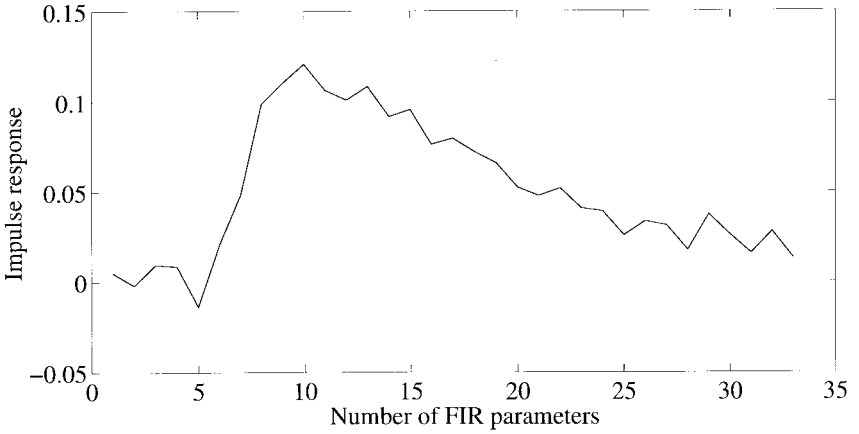

Fig. 15. The finite impulse response estimation of the first subprocess.

Minimizing a Loss Function: As shown in Section V-B, a subprocess can be satisfactory described by a first-order model. The following first-order OE model is used to determine the time delay of a subprocess

$$x_{n+1}(k) + f_1 x_n(k-1) = b_{n_k} x_n(k-n_k) + e(k) + f_1 e(k-1). \quad (20)$$

An estimate of the time delay is determined in a classical way by estimating parameters in (20) and by evaluating the loss function for different values of n_k, see Fig. 16. The time delay that corresponds to the minimal value of the loss function is chosen [15]. This technique is easy to use and it is less dependent on the noise compared to the other two methods, because the observed criterion is obtained by minimization of the prediction errors, therefore averaging the noise effects.

D. Static Gain and Bandwidth of the Subprocesses

In this section, a nonparametric identification technique is used to obtain an initial estimate of the subprocesses.

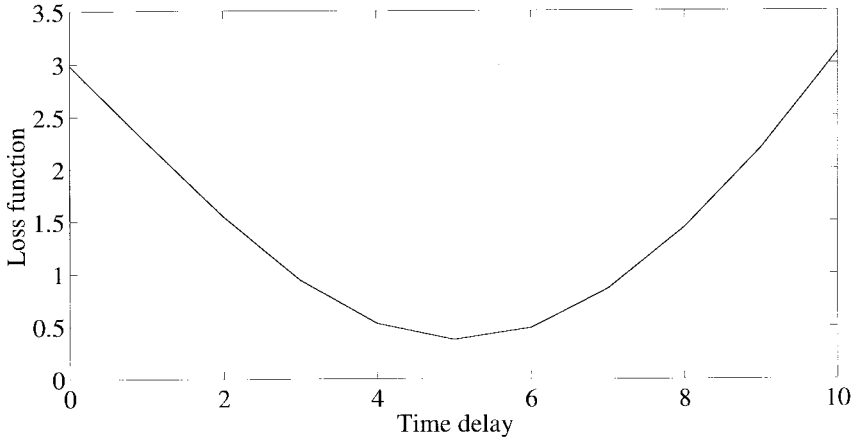

Fig. 16. The loss function with respect to the discrete-time delay n_k.

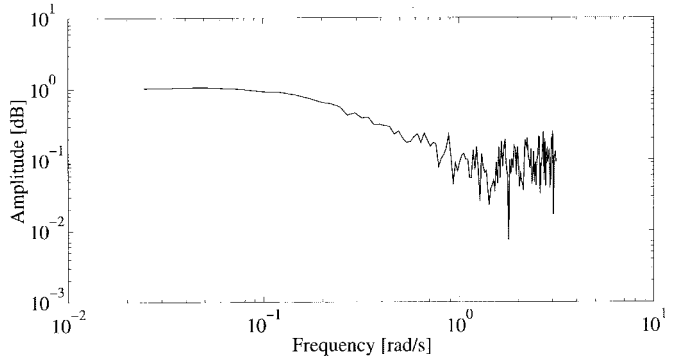

Fig. 17. Bode plot of the subprocess G_1.

TABLE I
THE PARAMETERS OF THE SECOND SUBPROCESS G_2; SEE FIG. 6

method	parameter b_0	parameter f_1 ($f_0 = 1$)	loss function
1	0.1676 ± 4.754e-3	-0.8371 ± 5.141e-3	0.4184
2	0.1804 ± 6.662e-4	-0.8072 ± 7.506e-4	0.4221
3	0.1562 ± 1.229e-2	-0.8346 ± 1.422e-2	0.6884
4	0.1706 ± 4.246e-3	-0.8335 ± 4.500e-3	0.4741
5	0.1718 ± 2.485e-3	-0.8326 ± 2.621e-3	0.2721

With spectral analysis the static gain and the bandwidth of a subprocess can be obtained [15]. Fig. 17 shows the results of spectral analysis of the first subprocess.

The static gain of the first subprocess is almost equal to one and the bandwidth is approximately 0.5 Hz. The other subprocesses yield similar results. The information obtained by spectral analysis are used to determine the sampling period and the appropriate filters for data preprocessing.

VI. APPLICATION OF THE FIVE STRATEGIES

In this section, the application of the five closed-loop identification strategies from Section IV on real-life data is discussed. The steering roll is excited with the generalized binary noise and the lateral strip positions are measured by cameras. To compare the five different strategies, the results at camera 3 (signal x_3) are shown. This signal is chosen deliberately, as the results for all the subprocesses are comparable. Refer to Fig. 1 for the definition of the camera locations and to the block diagram of Fig. 6 for the definition of different signals. Fig. 18 shows the measured lateral strip position x_1, and the input signal $\phi^{\mathrm{gbn}}(k)$ (without the control loop).

The signal $x_1(k)$ is influenced by two different effects. The high-frequency part is due to the GBN signal and the low-frequency part is a result of the mechanical feedback. First, the results of the three strategies without the control loop are compared and simulated with validation data.

Fig. 19 shows the results of strategy 1 (open-loop identification) which gives a rather accurate model. Strategies 2 and 3 yield slightly worse results in this case, see Table I for the numerical values of the estimated parameters and the related loss functions. As there is no remarkable difference in the true and simulated signals with respect to Fig. 19, the graphs are not shown here.

Second, the identification strategies of the experimental installation with the control loop are discussed. The deterministic disturbance due to the strip weld is suppressed by this loop. For this reason better results are expected with the following two strategies than with the previous ones. The fourth strategy is the application of the two-stage method on a system with two closed-loops. Fig. 20 shows the results of this strategy.

From Table I one can see that this method gives better results than the first three strategies. The last considered strategy is the CCCL. Because open-loop techniques are applied to a closed-loop system under the condition that the control loop is approximately equal to the mechanical loop, fewer identification stages are needed to identify the subprocesses. Since inaccuracies are introduced at each stage, fewer stages will in general give better results. The normalized error function $\epsilon(e^{j\omega})$ due to this approximation is shown in Fig. 12. The results of this strategy are given in Fig. 21, which shows an accurate approximation of the measured signal $x_3(k)$.

The results of the five identification strategies are summarized in Table I. In this table the parameters b_0 and f_1 of the

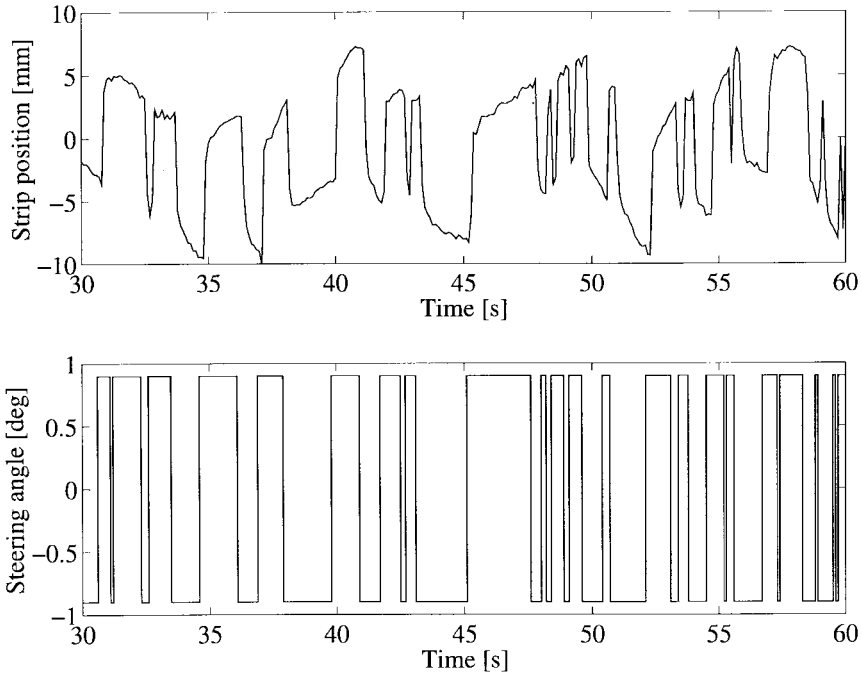

Fig. 18. Top: Measured signal x_1; bottom: Steering roll angle.

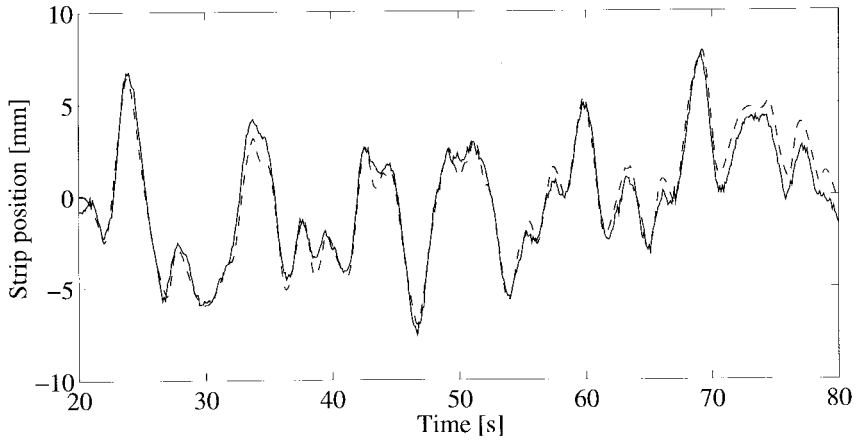

Fig. 19. Method 1 (open-loop identification): Measured (solid) and simulated (dashed) signal x_3.

OE model and the loss function [15] of the second subprocess G_2 are given. The parameter f_0 is equal to one.

The fifth method gives the lowest value of the loss function. This is because fewer stages are needed to identify the subprocesses, or formulated differently, because open-loop methods are directly applied in the absence of the deterministic disturbance. The results of the CCCL method are used to obtain a physically interpretable model of the experimental installation.

VII. A Physically Interpretable Model of the Installation

In this section, a physically interpretable model for the strip guidance process over cylindrical rolls is derived. The assumption made here is that the model parameters depend on the strip speed and tension. In Section VI, one can see that the subprocesses are very well represented by a first-order OE model

$$y(k) = q^{-n_k} \frac{b_0}{1 + f_1 q^{-1}} u(k). \tag{21}$$

To determine a physically interpretable model, nine different models are estimated, five for different strip speeds and five for different strip tensions

$$(v_s, \sigma_s) = [(v_1, \sigma_5), (v_2, \sigma_5), (v_3, \sigma_5), (v_4, \sigma_5), (v_5, \sigma_5) \\ (v_5, \sigma_4), (v_5, \sigma_3), (v_5, \sigma_2), (v_5, \sigma_1)].$$

The following first-order continuous-time model is used:

$$\frac{X_{n+1}(s)}{X_n(s)} = \frac{K}{1 + \tau s} e^{-T_d s}. \tag{22}$$

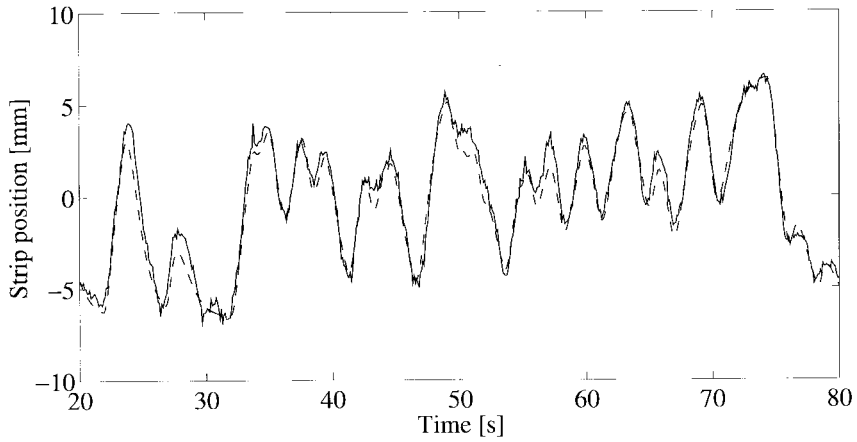

Fig. 20. Method 4 (two-stage method): Measured (solid) and simulated (dashed) signal x_3.

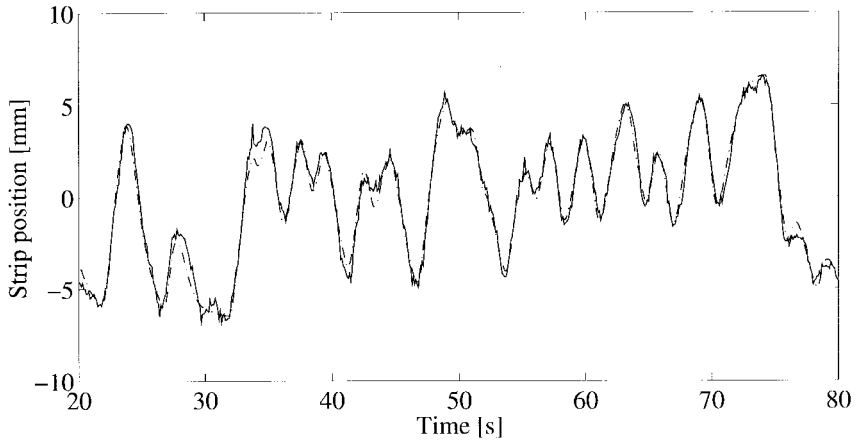

Fig. 21. Method 5 (CCCL): Measured (solid) and simulated (dashed) signal x_3.

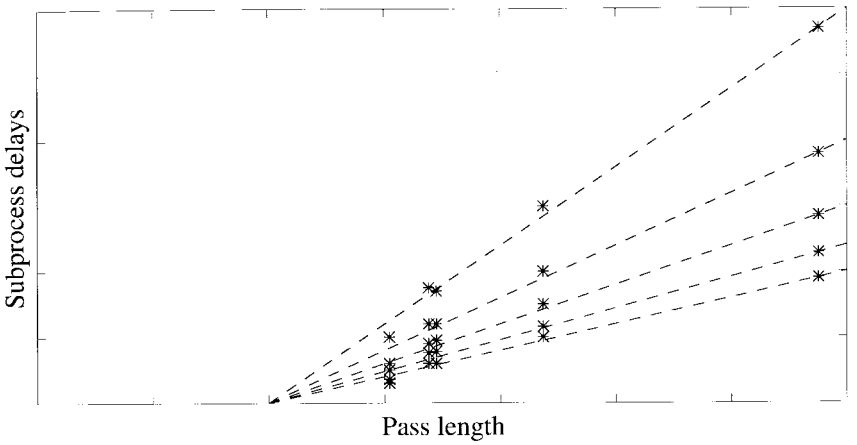

Fig. 22. The time delays with respect to the strip speed and the pass length.

The discrete-time parameters are translated to continuous time parameters by

$$\tau = \frac{T_s}{\ln\left(-\frac{1}{f_1}\right)} \quad K = \frac{b_0}{1+f_1}, \quad T_d = n_k T_s. \tag{23}$$

By plotting these parameters for all the models against the strip speed and the strip tension, the dependency of the model parameters can be examined. From the identification results, it can be concluded that there is no clear correlation between the time delays and the strip tension. Fig. 22 shows the time delays with respect to the pass length L_{pass} (see Fig. 4) and

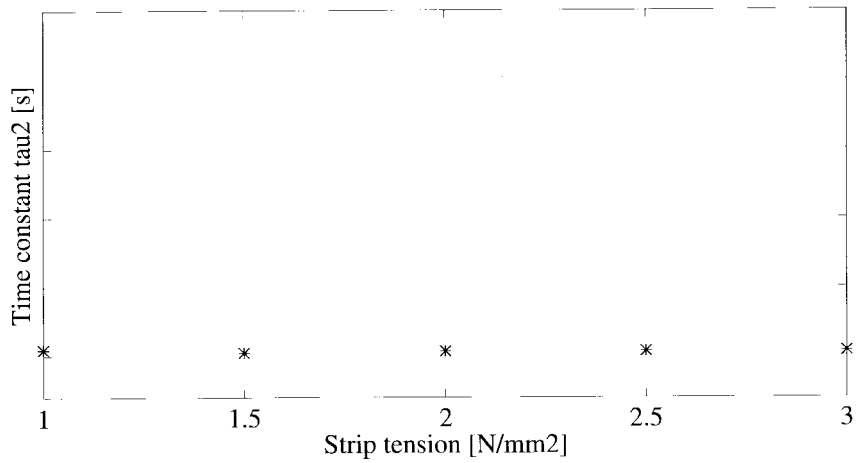

Fig. 23. Time constant of subprocess G_2 with respect to the strip tension.

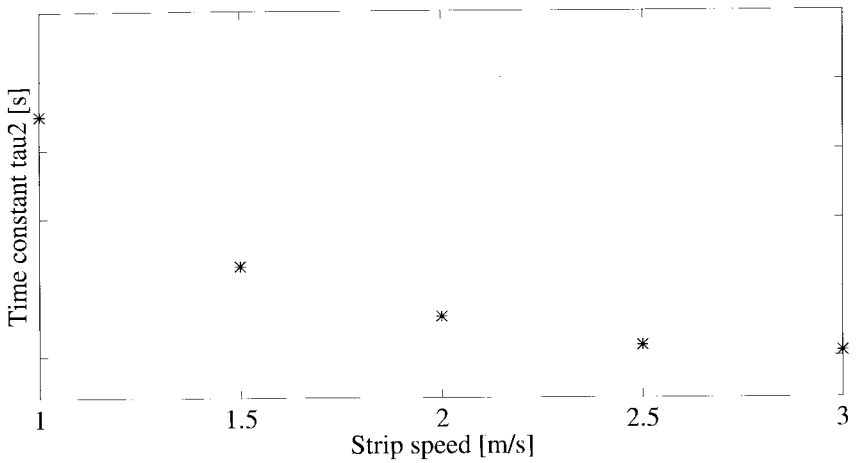

Fig. 24. Time constant of subprocess G_2 with respect to the strip speed.

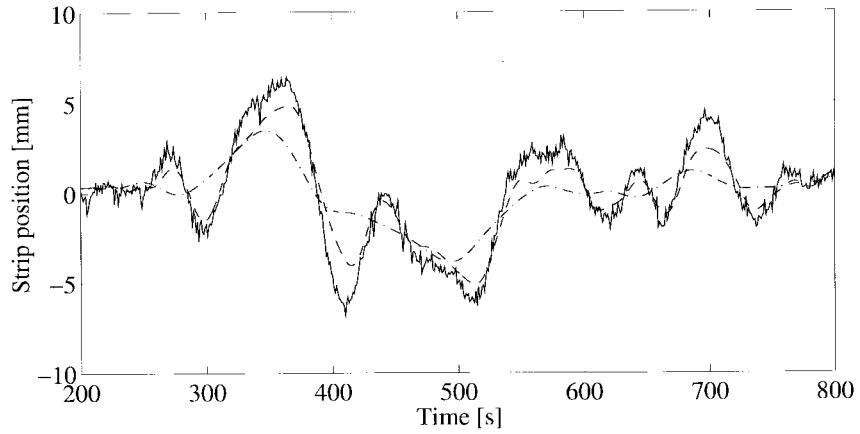

Fig. 25. Measured signal at camera 5 (solid) compared with the simulated signal x_5 of the obtained physical model (dashed) and the simulated signal of the model according Campbell [3] and Shelton [4] (dashed-dotted).

the strip speed. These time delays are compensated for the delay due to the roll, as indicated in (2). One can conclude that the linear approximations intersect the point $(L_0, 0)$, and the time delay of a subprocess can be approximated by

$$T_d = T_{\text{roll}} + \beta \frac{L_{\text{pass}} - L_0}{v_s} \tag{24}$$

with

L_0	empirically determined length [m];
L_{pass}	the pass length [m];
T_{roll}	the delay due to the roll [s], see (2);
T_d	the total time delay [s];
β	scaling constant.

Fig. 23 shows the time constant of the second subprocess with respect to the strip tension. Again, there is no remarkable dependency of the time constant on the strip tension.

Fig. 24 shows that the time constant depends on the strip speed, as is expected. The time constant, as a function of the strip speed, can be approximated by

$$\tau_n = \frac{\alpha_n}{v_s}. \tag{25}$$

The scaling constants α_n are for each subprocess obtained by least squares estimation. By observing the values of the constants α_n, no functional dependency in terms of the geometric parameters of the installation can be directly proposed as in the case of the time delays. This is a topic of further research.

The last parameter of the continuous model is the gain factor K. The identification results have shown that the gain factors are independent of the strip speed and tension and are very close to one. Hence, the gain is approximated by $K = 1$ for all subprocesses.

Finally, these results can be combined in a physically interpretable model of the experimental installation

$$\frac{X_{n+1}(s)}{X_n(s)} = \frac{K}{1+\tau s} e^{-T_d s} = \frac{1}{1+\frac{\alpha_n}{v_s}s} e^{-(T_{\text{roll}} + \beta \frac{L_{\text{pass}} - L_0}{v_s})s}. \tag{26}$$

To validate this model a special experiment is conducted under process conditions different from those used for the construction of the model. The strip speed v_s and the strip tension σ_s for validation are

$$v_3 < v_s < v_4 \quad \text{and} \quad \sigma_3 < \sigma_s < \sigma_4.$$

Again, the position at camera 5 of the installation is simulated. Four first-order models are connected in series. Fig. 25 shows the measured signal at camera 5 (solid line) and the simulated signal (dashed line) from our physically interpretable model. The simulated output from the model of Campell [3] and Shelton [4] (dashed-dotted line) is also plotted. It can be seen that the model derived in this article gives more accurate results.

VIII. Concluding Remarks

An experimental installation is used at Hoogovens to study the strip tracking behavior in processing lines. Contrary to these lines, this installation contains an internal feedback due to the use of an endless strip. To obtain results transferable from experiments with the experimental installation to the processing lines, an open-loop model of the experimental installation is needed. Application of the models from the literature to the experimental installation gives unsatisfactory results. Hence, closed-loop identification is used to obtain an open-loop model of the installation. Five different identification strategies are compared for one single operating condition and the strategy with the minimal prediction error (loss function) is selected to derive a physically interpretable model. The CCCL strategy proposed in this paper gives the minimal loss. The dependencies of the model parameters on the process parameters are examined and incorporated in a physically relevant model, which contains a few scaling constants. The scaling constant denoted α_n, related to the strip speed, requires further research to obtain a functional dependency in terms of geometric data of the installation. The derived model gives more accurate results of the strip guidance process through the experimental installation than the models described in [3] and [4].

References

[1] C. H. L. Limpens, "Impact of strip shape on strip tracking in a processing line," Hoogovens, IJmuiden, The Netherlands, Final Rep., no. 7; 7210-EA/604, 1995.

[2] "Fife Fach Symposium, Bandlaufregelanlagen in der Metallindustrie," Kelkheim, Germany, 1992 (in German).

[3] D. P. Campbell, *Process Dynamics*. New York: Wiley, 1958.

[4] J. J. Shelton and K. N. Reid, "Lateral dynamics of an idealised moving web," *ASME J. Dynamics, Syst., Measurement, Contr.*, vol. 93, no. 3, pp. 187–192, 1993.

[5] J. J. Shelton and K. N. Reid, "Lateral dynamics of a real moving web," *ASME J. Dynamics, Syst., Measurement, Contr.*, vol. 93, no. 3, pp. 180–186, 1993.

[6] I. Gustavsson, L. Ljung, and T. Söderström, "Identification of processes in closed-loop, identifiability and accuracy aspects," *Automatica*, vol. 13, pp. 59–75, 1977.

[7] P. M. J. van den Hof and R. J. P. Schrama, "An indirect method for transfer function estimation from closed-loop data," *Automatica*, vol. 29, pp. 1523–1527, 1993.

[8] M. Verhaegen, "Application of a subspace model identification technique to identify LTI systems operating in closed-loop," *Automatica*, vol. 29, pp. 1027–1040, 1993.

[9] H. J. A. F. Tulleken, "Generalized binary noise test-signal concept for improved identification experiment design," *Automatica*, vol. 26, no. 1, pp. 37–49, 1990.

[10] M. P. G. J. Besteman, "Identification of strip guidance installation," Hoogovens, IJmuiden, The Netherlands, Internal Rep. 84016, 1996 (in Dutch).

[11] B. A. Francis, *A Course in H_∞ Control Theory*. Berlin: Springer-Verlag, 1987.

[12] L. Ljung, *System Identification Toolbox—User's Guide*, The MathWorks, Inc., Natick, MA, 1991.

[13] M. Verhaegen, "Subspace model identification. Part I: The output-error state-space model identification class of algorithms," *Int. J. Contr.*, vol. 56, pp. 1187–1210, 1992.

[14] M. Verhaegen, R. M. C. Kraan, C. R. de Reus, A. P. J. van Rhijn, and H. B. Verbruggen, "Practical system identification in the process industry," *Contr. Comput.*, vol. 19, no. 1, 1991.

[15] L. Ljung, *System Identification, Theory for the User*. Englewood Cliffs, NJ: Prentice-Hall, 1987.

Marcel P. G. J. Besteman was born in Alkmaar, The Netherlands, on 2 February, 1968. He studied electrical engineering at the Technical University Delft, The Netherlands, where he received the Master's degree in 1996.

During his study, he worked as a technician at a canning factory. There he learned a lot about the practical aspects of technology and teamwork. In the final year of his study, he focused on system identification of open- and closed-loop systems. His main interest is the application of the control theory. Currently he works at Turnkiek Business Improvement B.V., The Netherlands. His main activity is the application of statistical process control in industry.

Camille H. L. Limpens was born in Maastricht, The Netherlands, on August 15, 1966. He studied applied physics at the Delft University of Technology, The Netherlands, where he received the Master's degree in 1989.

Since 1989 he has been a Researcher at the Research and Development Department of Koninklijke Hoogovens. His research interests until 1995 were the guiding of strips in processing lines. The last two years his main research interest has been the temperature control in rolling processes.

Robert Babuška was born in 1967 in Prague, Czechoslovakia. He received the M.Sc. degree in control engineering from the Czech Technical University in Prague in 1990 and the Ph.D. degree from the Delft University of Technology, The Netherlands, in 1997.

Currently, he is an Assistant Professor at the Control Laboratory of the Electrical Engineering Department, Delft University of Technology. His main research interests include identification and control of nonlinear systems, fuzzy set theory, and fuzzy systems modeling.

John B. Otten was born in 1959 in Emmen, The Netherlands, and received the B.Sc. degree from the Groningen Polytechnical College in 1982 and the M.Sc. degree from the University of Twente in 1987. Both degrees were obtained in mechanical engineering in, respectively, energy technology and technical mechanics and tribology.

In 1987, he was a Research Engineer at the Department of Rolling Mill Processes of Royal Dutch Hoogovens, the major Dutch steel and aluminum manufacturer. At the present he is Section Manager of the Mechatronics Department of Hoogovens Research and Development. One of the main research topics of this department involves the (static and dynamic) modeling as well as the experimental behavior of steel and aluminum webs for several continuous annealing and coating lines.

Michel Verhaegen (M'91) was born in Belgium on 2 September, 1959. He received the bachelor's degree in engineering/aeronautics from the Delft University of Technology, The Netherlands, in August 1982, and the doctoral degree in applied sciences from the Catholic University, Leuven, Belgium, in November 1985. During his graduate study, he held an IWONL research assistantship in the Department of Electrical Engineering.

From 1985 to 1987 he was a Postdoctoral Associate of the U.S. National Research Council and during that time was affiliated with the NASA Ames Research Center in California. From 1988 to 1989 he was an Assistant Professor at the Delft University of Technology, Department of Electrical Engineering. Since February 1990 he was a Senior Research Fellow of the Dutch Academy of Arts and Sciences and affiliated with the Network Theory Group of Delft University of Technology. From 1990 on, he has held short sabbatical leaves at the Universities of Uppsala, McGill, Lund, and the German Aerospace Research Center (DLR) in Munich. Currently he is an Associate Professor of the Delft University of Technology, Department of Electrical Engineering. His main research interest is the interdisciplinary domain of numerical linear algebra and system theory. Current activities focus on the development and practical application of subspace identification and the application of optimization and simulation tools in industrial controller design.

Dr. Verhaegen received a Best Presentation Award at the American Control Conference, Seattle, WA, 1986 and a Recognition Award from NASA in 1989. He is actively involved in the Dutch working group on software development of numerically reliable and efficient algorithms in system and control theory.